CHEMISTRY OF MATERIALS

ARTICLE

pubs.acs.org/cm

Structural Nature of Polyamorphism in $Y_2O_3-Al_2O_3$ Glasses

N. K. Nasikas,[†,§] S. Sen,[*,‡] and G. N. Papatheodorou[†]

[†]Institute of Chemical Engineering and High Temperature Chemical Processes, FORTH, P.O. Box 1414, GR-26504 Patras, Greece

[‡]Department of Chemical Engineering and Materials Science, University of California, Davis, California 95616, United States

[§]Department of Materials Science, University of Patras, GR-26504 Patras, Greece

ABSTRACT: The structural attributes of the polyamorphic high- and low-density amorphous phases in $Y_2O_3-Al_2O_3$ glasses with 24−41 mol % Y_2O_3 have been investigated using high-resolution ^{27}Al and ^{89}Y nuclear magnetic resonance spectroscopy in combination with back-scattered electron and transmission electron microscopy imaging and differential scanning calorimetric measurements. Glasses over the entire composition range are characterized by a uniform dispersion of droplets of one phase in the matrix of the other phase resulting from a density-driven phase separation in the supercooled liquid state. Although compositionally identical, the structures of the two phases differ primarily in their Y coordination environment and in the structural order associated with the connectivity and packing of the Al−O and Y−O coordination polyhedra. It appears that, compared to the matrix phase, the droplet phase is characterized by a significantly higher degree of short-range structural order.

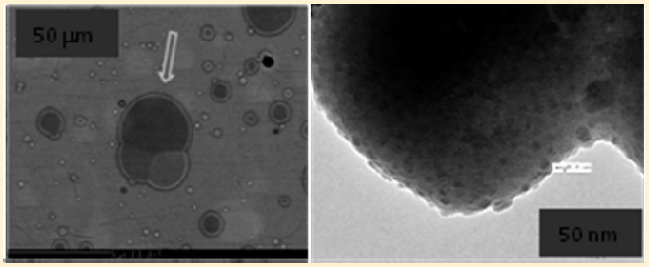

KEYWORDS: $Y_2O_3-Al_2O_3$, glass, supercooled liquid, polyamorphism, structure, nuclear magnetic resonance, ^{27}Al, ^{89}Y, differential scanning calorimetry, transmission electron microscopy

INTRODUCTION

Crystalline and amorphous rare earth aluminates constitute an important class of optical materials with a wide range of technological applications.[1−3] Particularly noteworthy in this regard is the crystalline yttrium aluminum garnet (YAG; $Y_3Al_5O_{12}$) in the $Y_2O_3-Al_2O_3$ binary system that is known for its profound importance as a host material in solid state lasers.[3−7] More recently, glasses and supercooled liquids in this binary system have been extensively investigated in relation to the observation of a density-driven first-order liquid−liquid phase transition.[8−26] The existence of this type of phase transition is a fundamental and currently greatly debated issue in the literature, i.e., whether, similar to crystalline polymorphs, two or more isocompositional glass or liquid phases with different structures and densities that are in stable or metastable equilibrium could coexist. Such a phenomenon has been termed polyamorphism in the literature.[27] In the very first report by Aasland and McMillan,[8] $Y_2O_3-Al_2O_3$ glasses were prepared in the composition range of 24−32 mol % Y_2O_3 by melting the mixture of the constituent oxides in an inert atmosphere in a modified iridium wire furnace. For every glass prepared in this compositional range, these authors observed glassy inclusions of several micrometers embedded in a glassy matrix using back-scattered electron (BSE) imaging. These authors verified using electron probe microanalysis that the inclusions as well as the matrix had the same composition. Micro-Raman spectroscopy was employed to demonstrate structural differences between these two phases in the glass samples. These results led to the conclusion that the inclusion and the matrix represented two thermodynamically distinct but compositionally identical amorphous phases. The inclusions were assigned to the low-density amorphous (LDA) phase, and the surrounding matrix phase was assigned to the high-density amorphous (HDA) phase, related via a first-order liquid−liquid phase transition.

Subsequent studies have used CO_2 laser melting and containerless aerodynamic levitation to prepare these glasses.[9−22] The results of these studies are generally in agreement that the observability of the coexistence of HDA and LDA phases with BSE may be a critical function of glass composition. The composition range of 25−33 mol % Y_2O_3 is more favorable for the production of single-phase glasses, whereas two-phase glasses form in the composition range of 33−40 mol % Y_2O_3.[13,18,21,22] These results are in contrast with the observation of two-phase glasses by Aasland and McMillan[8] in the composition range of 24−32 mol % Y_2O_3. Such a discrepancy may possibly arise from the difference in the synthesis techniques and hence in the thermal history of these glasses, as mentioned above. Structural studies of these glasses in the composition range of 24−40 mol % Y_2O_3 were conducted by several laboratories using primarily ^{27}Al nuclear magnetic resonance (NMR) spectroscopy and X-ray and neutron diffraction. All $Y_2O_3-Al_2O_3$ glasses in this composition range showed the presence of Al atoms in 4-, 5-, and 6-fold coordination forming AlO_4, AlO_5, and AlO_6 coordination polyhedra, respectively. The relative fractions of these Al species have been shown to be relatively insensitive to the glass composition.[13] The diffraction results have been interpreted to indicate that on an average the Y atoms are six- or seven-coordinated with respect to oxygen in these

Received: January 24, 2011
Revised: March 29, 2011
Published: May 13, 2011

dx.doi.org/10.1021/cm200241c | *Chem. Mater.* 2011, 23, 2860–2868

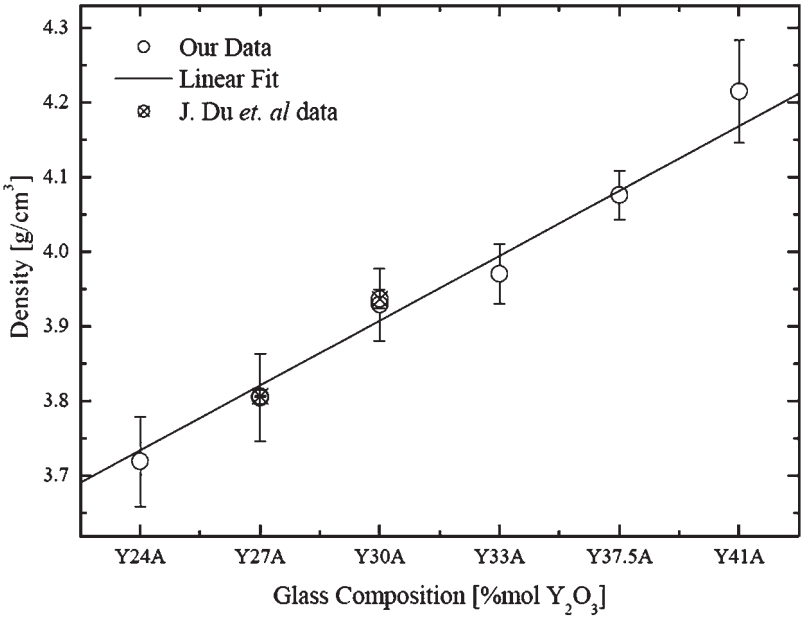

Figure 1. Densities of $Y_2O_3-Al_2O_3$ glasses (○) as determined in this study. The straight line is a linear least-squares fit to our data. Circles with crosses represent data on two compositions from ref 21.

glasses with some small fraction of Y being eight-coordinated near the YAG composition.[12,20] Wilding and McMillan[10−12] used differential scanning calorimetry (DSC) to further investigate the thermodynamic differences between the HDA and LDA phases for glasses containing 20−32 mol % Y_2O_3. The DSC results revealed a glass transition temperature T_g at ∼1135 K, and additionally, the presence of a second T_g was observed at 1300 K for the 24 mol % Y_2O_3 glass. These two T_g values were somewhat arbitrarily attributed to the HDA and LDA phases, respectively. It should be noted that McMillan and Wilding[23] managed to mechanically separate the HDA and LDA phases of these glasses and reported their densities to be 3.72 and 3.58 g/cm^3, respectively, as measured by the sink−float technique.

More recently, Greaves and co-workers[24,26] combined in situ high-temperature small angle X-ray scattering (SAXS) and wide angle X-ray scattering (WAXS) along with aerodynamic levitation to study the liquid−liquid phase transitions in a $Y_2O_3-Al_2O_3$ liquid with 20 mol % Y_2O_3. At very high temperatures (>1700 K), the yttrium aluminate melts displayed a narrow and reversible maximum in the SAXS signal that was interpreted as an indication of liquid unmixing at a nanometer length scale, associated with liquid−liquid phase transition. This result was corroborated with the observation of an abrupt realignment in WAXS patterns, related to reversible shifts in polyhedral packing on the atomic scale. Following this work, Barnes et al.[25] performed high-energy X-ray diffraction, small angle neutron scattering, and pyrometry studies on aerodynamically levitated samples in the composition range of 20−37.5 mol % Y_2O_3. However, these authors were unable to confirm the findings of the previous work by Greaves and co-workers[24,26] as no clear evidence of a liquid−liquid phase transition was observed in the levitated $Y_2O_3-Al_2O_3$ liquid with 20 mol % Y_2O_3.

It is clear that although this glass-forming system has been extensively studied in relation to the observability of liquid−liquid phase transition or polyamorphism, the exact nature of the structural differences between the two polyamorphic phases in these glasses has remained controversial and speculative at best. In previous studies, it has been variously ascribed to the differences in the coordination environments of Y and/or Al atoms and in the metal−metal correlations.[9,16−20] This issue holds the key to our understanding of the resulting differences in the thermodynamic properties and consequently the origin of polyamorphism in these glass-forming liquids. Here we report the results of a comprehensive study of $Y_2O_3-Al_2O_3$ glasses with 24−41 mol % Y_2O_3 prepared by containerless aerodynamic levitation and CO_2 laser melting, using a combination of ^{27}Al and ^{89}Y magic-angle-spinning (MAS) NMR spectroscopy, DSC, BSE, and transmission electron microscopy (TEM) imaging and density measurements. Our results provide for the first time direct and quantitative information about the structural differences between the polyamorphic phases in yttrium aluminate glasses.

EXPERIMENTAL DETAILS

Synthesis and Physical Characterization. The $Y_2O_3-Al_2O_3$ glass samples were prepared from high-purity (99.999%, Alfa Aesar) constituent oxides as starting materials. Both Y_2O_3 and Al_2O_3 powders were dried in a neutral atmosphere at ∼400 °C for approximately 24 h and subsequently were transferred to a water-free glovebox. Stoichiometric amounts of these two oxides corresponding to compositions with 24, 27, 30, 33, 37.5, and 41 mol % Y_2O_3 were carefully weighed and mixed by grinding with a pestle and mortar. These batches were doped with 0.1 wt % Gd_2O_3 to shorten the ^{89}Y NMR spin−lattice relaxation time. The formation of glass by these mixtures was achieved in two steps. First, small amounts of the powder mixtures were placed on a water-cooled copper hearth for melting with the use of a 240 W CO_2 laser (Synrad Evolution Series), operating at 10.6 μm. The laser power was gradually and carefully increased until the samples completely melted. The percentage of the laser power did not exceed ∼15% to avoid temperatures far above the liquidus that could alter the composition due to evaporation. Samples were carefully heated to a maximum of 100 K above liquidus such that no evaporation of oxide was observed on the wall of the protective quartz tubing surrounding the levitated sample.

dx.doi.org/10.1021/cm200241c |*Chem. Mater.* 2011, 23, 2860–2868

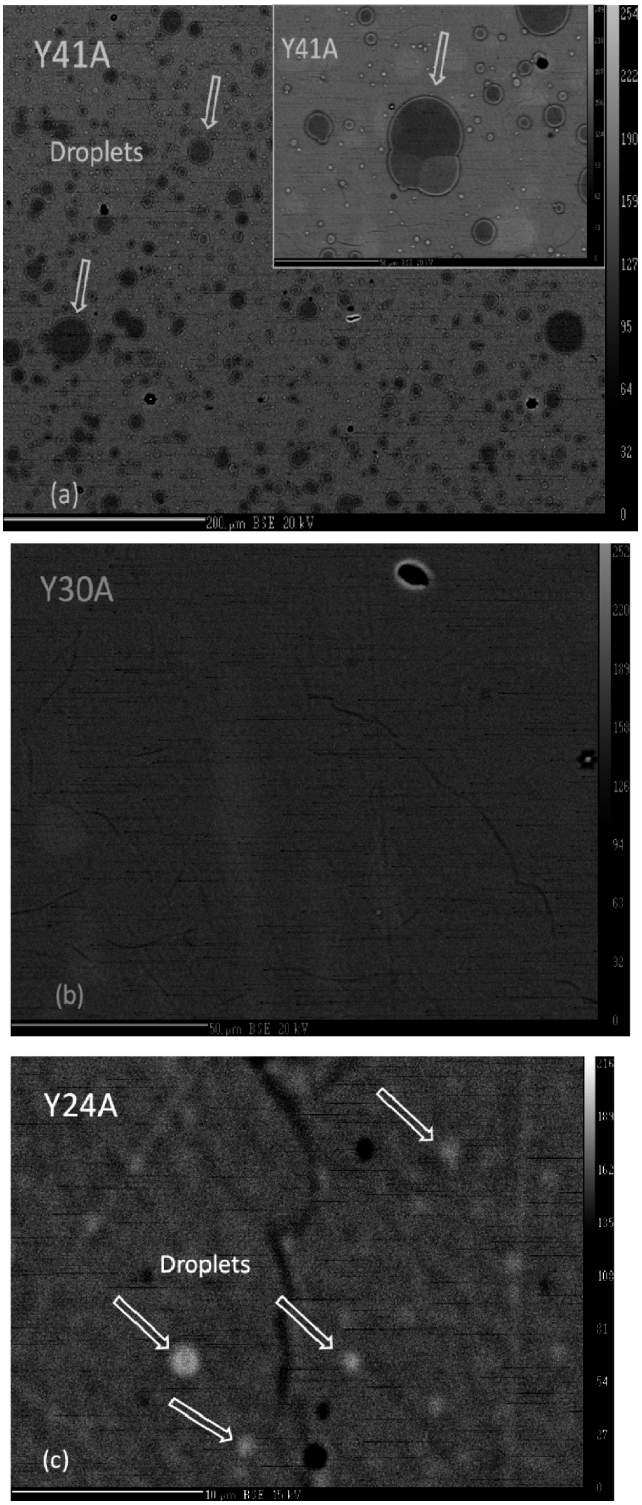

Figure 2. BSE images of $Y_2O_3-Al_2O_3$ glasses with 41, 30, and 24 mol % Y_2O_3 (from top to bottom, respectively). Arrows in the top and bottom images indicate the droplet phase. White bars at the bottom left corners correspond to lengths of 200, 50, and 10 μm for the images from top to bottom, respectively. The inset in the top image is a magnified view of a composite droplet formed via collapse of at least three smaller droplets. The white bar at the bottom left corner of the inset denotes a length scale of 50 μm.

The protective tube was observed to be covered by a thin white film of oxide in case of accidental overheating of the melt, in which case the corresponding glass sample was discarded. Sudden shut down of the laser yielded polycrystalline and nearly spherical beads. The second step was to aerodynamically levitate these spherical beads by using a controlled flow of Ar gas through a conical nozzle and to carefully remelt these beads using the CO_2 laser.[28] Subsequent sudden shutdown of the CO_2 laser yielded spherical, completely colorless, and transparent amorphous materials ~1.5−2 mm in diameter.

For every composition, ~20−30 glassy spheres were prepared. All spheres were found to be X-ray amorphous. Furthermore, "quick" Raman spectra were recorded for each glass sphere using a commercial micro-Raman spectrometer (Labram HR 800 equipped with a He−Cd laser) operating at 441.6 nm. The details of the Raman spectroscopic results will be reported in a future publication; however, these spectra displayed broad bands without any sharp peaks expected from crystalline phases, thus confirming the amorphous character of the glass beads.

The chemical compositions of all glasses as reported here were analyzed with the standard electron probe microanalysis (EPMA) technique (CAMECA SX-100) and were found to be the same as the nominal compositions to within ±0.1 mol %. All glasses were found to be chemically homogeneous over length scales of a few micrometers, the latter being limited by the resolution of the electron probe microanalysis (EPMA) technique. T_g and the crystallization onset temperatures of $Y_2O_3-Al_2O_3$ glasses with 24, 30, and 41 mol % Y_2O_3 were determined within ±2 K by differential scanning calorimetry (SETSYS Evolution TGA-DTA/DSC) using a heating rate of 40 K/min, and density was determined by the Archimedes method using toluene as the immersion medium. A few beads of the glass sample with 30 mol % Y_2O_3 were crushed into small pieces that were subsequently mounted in epoxy, thin sectioned using a diamond knife to a thickness of approximately 70 nm, and mounted onto 300 mesh copper grids with a carbon/Formvar substrate for imaging using a high-resolution transmission electron microscope (JEOL JEM2500SE) to investigate the existence and length scale of any spatial inhomogeneity in the sample density.

NMR Spectroscopy. The ^{27}Al and ^{89}Y MAS NMR spectra were recorded using a Bruker Avance 500 spectrometer and Bruker magnet (11.7 T) operating at Larmor frequencies of 24.5 and 130.3 MHz for ^{89}Y and ^{27}Al, respectively. A low-γ Bruker 4 mm MAS probe was used to collect the ^{89}Y MAS NMR data; crushed samples were spun at 8 kHz, and free induction decays (FIDs) were collected using a $\pi/2$ radio-frequency pulse (6 μs) and a recycle delay of 5 s. The probe ring-down time of ~75 μs was short enough that significant distortion of the ^{89}Y NMR line shape could be avoided. Approximately 30000−50000 FIDs were averaged and Fourier-transformed to obtain each ^{89}Y MAS NMR spectrum. For one of the samples, an ^{89}Y MAS NMR spectrum was collected with a recycle delay of 20 s. This spectrum did not display any noticeable difference in the line shape compared to that obtained with a recycle delay of 5 s, thus indicating the absence of any significant differential relaxation. ^{89}Y NMR chemical shifts were referenced to that of crystalline $Y_2Sn_2O_7$ (δ_{iso} = 150 ppm). ^{27}Al MAS NMR spectra were recorded using a Bruker triple-resonance 2.5 mm MAS probe; crushed samples were spun at 33 kHz, and FIDs were collected using a $\pi/9$ solid radiofrequency pulse (0.4 μs) and a recycle delay of 0.5 s. Longer delays of up to 2 s did not result in appreciably different data. Approximately 10000−15000 FIDs were averaged and Fourier-transformed to obtain each ^{27}Al MAS NMR spectrum.

^{27}Al triple-quantum MAS (3QMAS) NMR spectra were recorded for two glass compositions with 27 and 41 mol % Y_2O_3 using a three-pulse zero quantum filtered pulse sequence. Samples were spun using a Bruker triple-resonance 2.5 mm MAS probe at a rate of 33 kHz. The high-power (ν_{RF} = 140 kHz) excitation and conversion pulse lengths were optimized to 3.6 and 1.1 μs, respectively. The pulse length for the $\pi/2$ selective pulse was 12 μs. 3QMAS data were typically collected using 500−1000 acquisitions with a recycle delay of 0.5−2 s at each of the 128 t_1 slices. These slices were spaced in increments of a full rotor cycle of 30.3 μs.

Table 1. Chemical Compositions of the Droplet and Matrix Phases in Y_2O_3–Al_2O_3 Glasses

	nominal bulk composition (mol %)		droplet phase composition		matrix phase composition (±0.1 mol %)	
sample	Y_2O_3	Al_2O_3	Y_2O_3	Al_2O_3	Y_2O_3	Al_2O_3
Y41A	41.0	59.0	40.2 ± 0.1 mol %	59.8 ± 0.1 mol %	40.4 ± 0.1 mol %	59.6 ± 0.1 mol %
			59.7 ± 0.08 wt %[a]	40.1 ± 0.10 wt %[a]	59.8 ± 0.10 wt %[a]	40.1 ± 0.09 wt %[a]
Y24A	24.0	76.0	23.7 ± 0.1 mol %	76.3 ± 0.1 mol %	23.9 ± 0.1 mol %	76.1 ± 0.1 mol %
			40.7 ± 0.10 wt %[a]	59.1 ± 0.06 wt %[a]	40.9 ± 0.08 wt %[a]	58.9 ± 0.10 wt %[a]

[a] Oxide concentrations reported in weight percent are the raw microprobe data. Each analysis is an average of data taken at 10 randomly chosen points in three randomly chosen glass spheres for each sample.

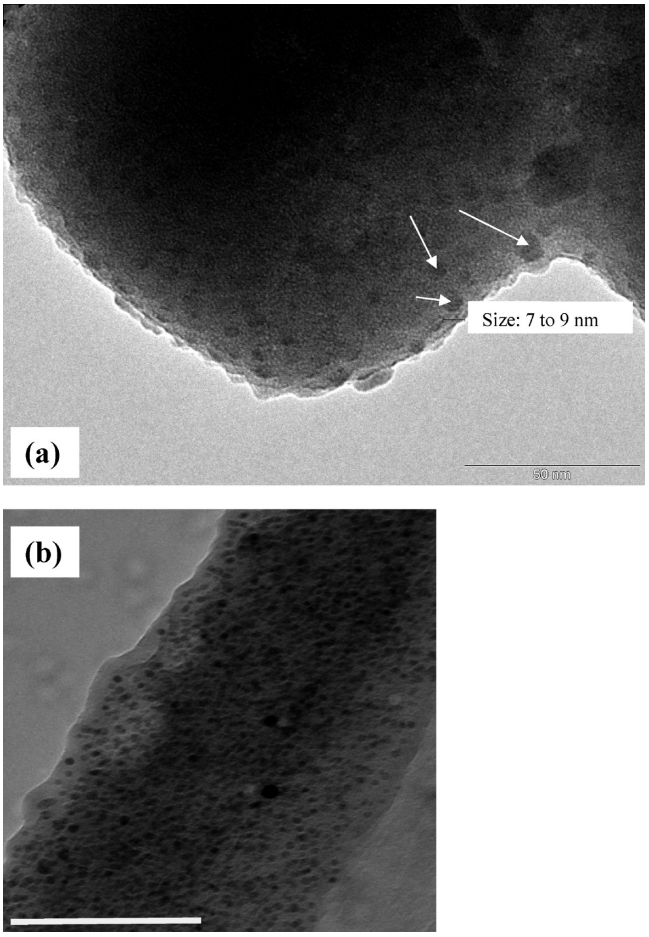

Figure 3. (a) TEM image of Y_2O_3–Al_2O_3 glass with 30 mol % Y_2O_3 taken at a magnification level of 700000×. White arrows show nearly spherical droplets with average diameters of ∼7−9 nm. (b) TEM image of the same sample as in panel a, taken at a lower magnification (the white bar at the bottom corresponds to 100 nm).

The ^{27}Al 3QMAS spectra were processed and shear transformed using Bruker TopSpin software. All ^{27}Al chemical shifts were externally referenced to a 1 M aqueous solution of $Al(NO_3)_3$.

RESULTS

Results from the density measurements for these glasses are shown in Figure 1. The average density increases nearly linearly with an increasing Y_2O_3 content in these glasses (Figure.1). The glass densities determined in this study are in good agreement with the results reported for select compositions in previous studies.[20,21] Back-scattered electron (BSE) images for glasses with 24, 30, and 41 mol % Y_2O_3 were collected with the EPMA setup and are shown in Figure 2. The BSE image for the glass with 41 mol % Y_2O_3 clearly shows the presence of droplets with sizes ranging from a few micrometers to 50 μm, dispersed in a matrix. It is clear from these BSE images that some of the larger droplets are formed by the coalescence of smaller droplets (see the inset of Figure 2a). Such droplets are also observed in the BSE image of the glass with 24 mol % Y_2O_3; however, these droplets are significantly smaller ($\leq$1 μm) than those characteristic of the 41 mol % Y_2O_3 glass (Figure 2). The lighter or darker appearance of the droplets compared to the matrix in these BSE images implies density differences between these two phases. Electron probe microanalyses of the droplet and matrix phases in these glasses show that the chemical compositions of these two phases are practically identical (see Table 1). In contrast, the BSE image of the glass with 30 mol % Y_2O_3 does not show the presence of any droplet phase (Figure 2). However, the high-magnification TEM image of this glass clearly reveals the presence of nearly monodisperse and spherical ∼7−9 nm droplets (Figure 3).

The DSC thermograms for Y_2O_3–Al_2O_3 glasses with 24, 30, and 41 mol % Y_2O_3 are shown in Figure 4. Previous studies, most notably by Wilding and McMillan,[10−12] reported the presence of two T_g values in the DSC thermograms of Y_2O_3–Al_2O_3 glasses. For example, in the case of the glass with 24 mol % Y_2O_3, these authors observed two T_g values at ∼1135 and 1300 K. The DSC thermogram for the glass with 41 mol % Y_2O_3 acquired in this study clearly displays the presence of two T_g values with onset temperatures near 1160 and 1270 K with an intervening exothermic peak near 1220 K (Figure 4). This exothermic peak possibly corresponds to the crystallization of the YAG phase considering the compositional similarity of the latter (37.5 mol % Y_2O_3) with that of the bulk glass. In contrast, the DSC thermogram for the glass with 30 mol % Y_2O_3 displays a single T_g with an onset temperature of ∼1160 K followed by a crystallization exotherm centered at ∼1255 K (Figure 4). The glass with 24 mol % Y_2O_3 displays a clear glass transition with an onset temperature of ∼1160 K and two crystallization events with exotherms centered near 1240 and 1270 K. There is another signature of a possible glass transition in the DSC thermogram of this glass with an onset temperature near 1300 K. However, strong overlap of this T_g signal with the tail of the second crystallization exotherm at 1270 K makes it less convincing than the case for the 41% Y_2O_3 glass for which the second T_g is clearly resolved in the DSC thermogram (Figure 4).

The ^{27}Al MAS NMR spectra of glasses with 24, 33, and 41 mol % Y_2O_3 are shown in Figure 5. In spite of significant overlap, these spectra clearly reveal three distinct resonances that peaked at ∼60, ∼38, and ∼10.6 ppm, corresponding to Al in 4-, 5-, and

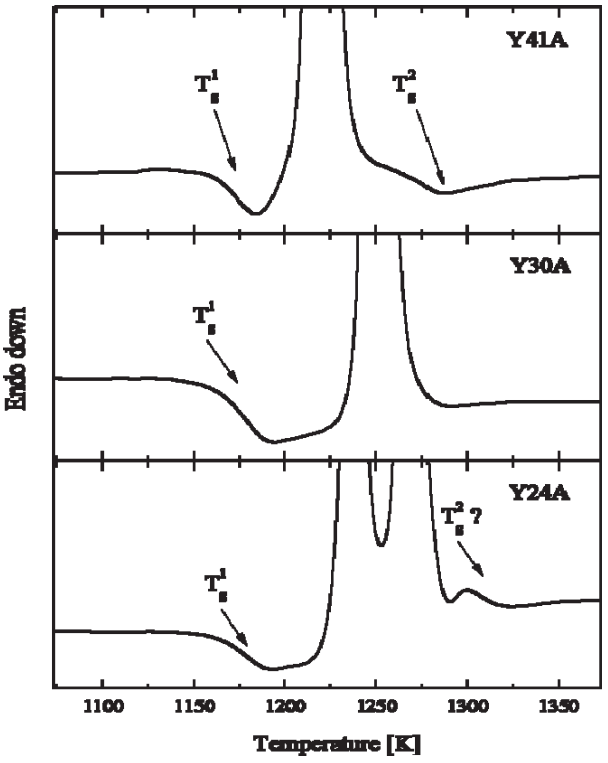

Figure 4. DSC thermograms of $Y_2O_3-Al_2O_3$ glasses with 41, 30, and 24 mol % Y_2O_3 (from top to bottom, respectively). Arrows indicate the onset of glass transitions. Exothermic peaks (off scale) represent crystallization events.

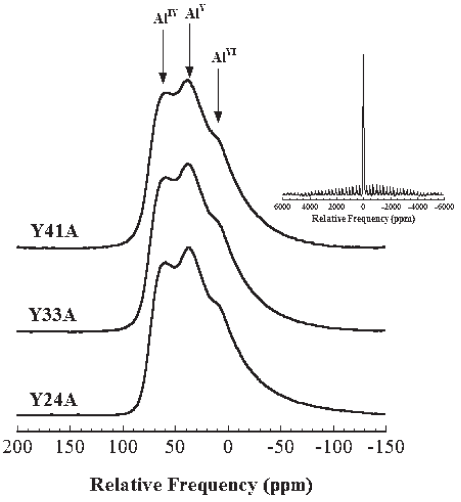

Figure 5. ^{27}Al MAS NMR spectra of $Y_2O_3-Al_2O_3$ glasses with 41, 30, and 24 mol % Y_2O_3. Corresponding glass compositions are denoted alongside each spectrum as Y#A, where the # denotes the Y_2O_3 content in mole percent. The inset shows the full view of the spectrum (over the complete sweep width) of the Y30A sample, including the spinning side bands.

6-fold coordination, respectively, with oxygen (Al^{IV}, Al^{V}, and Al^{VI}, respectively). The line shapes and relative intensities of these resonances do not appear to change significantly with glass composition (Figure 5). These results are completely consistent with detailed ^{27}Al NMR results for $Y_2O_3-Al_2O_3$ glasses reported in previous studies.[11,13,15,21,27,29,30] The absence of any sharp resonance in the ^{27}Al MAS NMR spectra in Figure 5 confirms the amorphous nature of these samples as the expected and commonly encountered crystalline phases in these glasses, namely, YAG, Al_2O_3, and $YAlO_3$, are all characterized by rather narrow ^{27}Al resonances.[15] On the other hand, the possibility of the presence of small amounts of (a) crystalline phases that are characterized by broad ^{27}Al MAS NMR line shapes and/or (b) nanometer-sized crystals with sizable structural disorder cannot be completely discarded on the basis of our ^{27}Al NMR data.

The Al^{IV}, Al^{V}, and Al^{VI} resonances in the ^{27}Al MAS NMR spectra are completely resolved in the ^{27}Al 3QMAS spectra of these glasses (Figure 6). These ^{27}Al 3QMAS spectra are similar to that reported previously by Tangeman et al. for a glass of YAG composition with 37.5 mol % Y_2O_3.[15] A comparison between the ^{27}Al 3QMAS spectra of the two glasses with 24 and 41 mol % Y_2O_3 in Figure 6 does not show any significant differences. The isotropic chemical shifts and the quadrupolar product P_q for the Al^{IV}, Al^{V}, and Al^{VI} species can be calculated from these 3QMAS NMR spectra using the procedures described by Amoureux et al.[31] For each resonance in the 3QMAS NMR spectrum, the centers of gravity in the MAS and isotropic dimensions (δ_2^{CG} and δ_{iso}^{CG}, respectively) are used to calculate the isotropic chemical shift δ_{CS} and the quadrupolar coupling product (P_q) according to

$$\delta_{CS} = \frac{10}{27}\delta_2^{CG} + \frac{17}{27}\delta_{iso}^{CG} \quad (1)$$

and

$$P_q = (\delta_{iso}^{CG} - \delta_2^{CG})^{1/2} \times f(I) \times \nu_0 \times 10^{-3} \quad (2)$$

where $f(I) = 10.244$ for $I = {}^5/_2$ nuclides.[31] Calculations on the basis of eq 1 and the experimental values of δ_2^{CG} and δ_{iso}^{CG} for the Al^{IV}, Al^{V}, and Al^{VI} peaks in the ^{27}Al 3QMAS spectra yield δ_{CS} values of 75.9, 44.4, and 10 ppm, respectively, for these three Al sites. On the other hand, the application of eq 2 results in P_q values of ~4.4, 3.5, and 0 MHz for the Al^{IV}, Al^{V}, and Al^{VI} sites, respectively. Because $P_q = C_q(1 + \eta^2/3)^{1/2}$, where C_q is the quadrupolar coupling constant and η $(0 \le \eta \le 1)$ is the asymmetry parameter of the electric field gradient tensor at the Al sites, the P_q values mentioned above provide an upper bound for C_q (when $\eta = 0$), whereas the lower bound would be a value that is 15% lower, corresponding to $\eta = 1$. It is important to note that the resonances for the Al^{IV} and Al^{V} sites in the ^{27}Al 3QMAS NMR spectra in Figure 6 show contours of intensities that are elongated away from the diagonal along which the condition $\delta_2^{CG} = \delta_{iso}^{CG}$ is satisfied while the intensity of the Al^{VI} site is primarily concentrated on the diagonal. This result is consistent with the P_q values determined for the various Al sites as it indicates that the Al^{IV} and Al^{V} sites are characterized by strong quadrupolar interaction, while in comparison, the Al^{VI} site is broadened primarily via chemical shift distribution and the quadrupolar effect is negligible.

The δ_{CS} values mentioned above are in good agreement with the average δ_{CS} values of 75.1, 44.8, and 11.3 ppm for Al^{IV}, Al^{V}, and Al^{VI} sites, respectively, in $Y_2O_3-Al_2O_3$ glasses as reported in a previous study by Tangeman et al. on the basis of high-field ^{27}Al MAS NMR line shape analyses.[15] The same set of analyses by Tangeman et al. resulted in C_q values of 9.5, 8.6, and 5.8 MHz for the Al^{IV}, Al^{V}, and Al^{VI} sites, respectively. It is to be noted that these C_q values are significantly higher than the P_q values of ~4.4, 3.5, and 0 MHz, respectively, mentioned above as obtained from

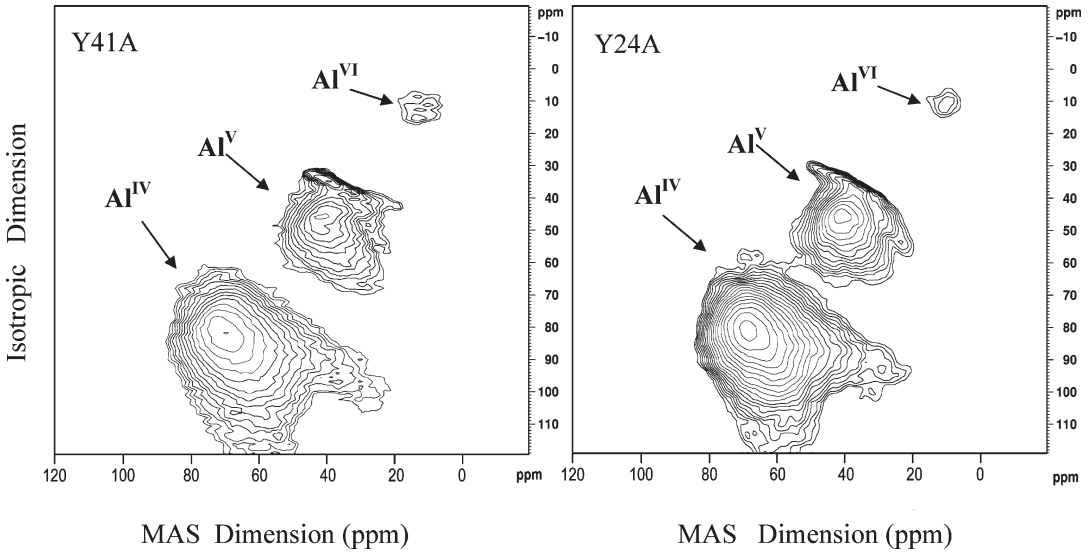

Figure 6. ^{27}Al 3QMAS NMR spectra of $Y_2O_3-Al_2O_3$ glasses with 41 (left) and 24 mol % Y_2O_3 (right).

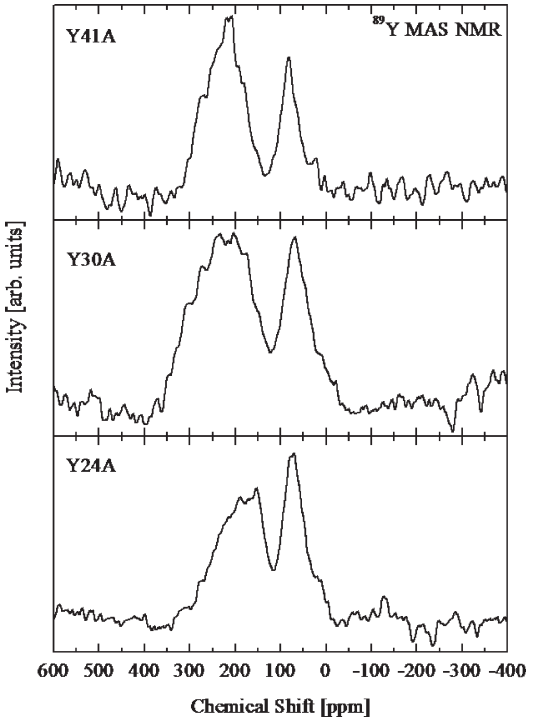

Figure 7. ^{89}Y MAS NMR spectra of $Y_2O_3-Al_2O_3$ glasses with 41, 30, and 24 mol % Y_2O_3 (from top to bottom, respectively).

the ^{27}Al 3QMAS NMR spectra in Figure 6. A corresponding discrepancy between the ^{27}Al MAS and 3QMAS NMR line shapes was also noted by Tangeman et al. and was attributed to the well-known problem of preferential excitation of sites with smaller C_q values in multiple-quantum MAS (MQMAS) NMR over those with larger ones.[15]

Unlike ^{27}Al NMR spectra, the ^{89}Y NMR spectra of glasses in this binary system have never been reported in the literature. The ^{89}Y MAS NMR spectra of glasses with 24, 30, and 41 mol % Y_2O_3 are shown in Figure 7. It is clear from these spectra that the Y atoms occupy at least two distinct sites in all glasses that are manifested as a broad ^{89}Y resonance spanning the range of 110−300 ppm and a narrow resonance centered near 75 ppm. Intensities corresponding to the spinning side bands are not observed in these spectra. The center of gravity of the broad resonance shifts from near 175 ppm for the glass with 24 mol % Y_2O_3 to near 208 and 220 ppm for the glasses with 30 and 41 mol % Y_2O_3, respectively. Simulations of these ^{89}Y MAS NMR spectra with Gaussian line shapes seem to indicate that the relative fraction of the narrow peak decreases from 33% for the glass with 24 mol % Y_2O_3 to 28% for the glass with 30 mol % Y_2O_3 and reaches a minimum value of 25% for the glass with 41 mol % Y_2O_3. However, it should be noted that the experimental error bar associated with these relative fractions is rather large, ∼3%.

DISCUSSION

It is important to stress at the outset that unlike a number of previous reports in the literature,[14,15,22,32] the $Y_2O_3-Al_2O_3$ glasses that are prepared in this study appear to be practically free of any crystalline inclusions that can be detected using XRD, Raman, and NMR spectroscopic techniques over the entire composition range of 24−41 mol % Y_2O_3. The BSE images and DSC results, when taken together, unambiguously indicate the presence of two glassy phases with different densities and glass transition temperatures but with practically identical chemical compositions in the case of the glass with 41 mol % Y_2O_3. The morphology of the droplet phase indicates their formation via nucleation rather than via spinodal decomposition in the supercooled liquid state (Figure 2). Significantly smaller droplets have also been observed in the glass with 24 mol % Y_2O_3, consistent with the possible presence of two T_g values in its DSC thermogram (Figure 4). Therefore, the coexistence of the droplet and the matrix phases with identical composition but different densities in these glasses implies a density-driven phase separation consistent with the concept of polyamophism.[8−11,15−18,23,26,27,33] On the other hand, both BSE imaging and DSC scanning indicate the presence of a single glass phase in the sample with 30 mol % Y_2O_3. However, TEM imaging reveals the presence of ∼7−9 nm spherical droplets in this sample, implying that the observability of the droplets in this glass by BSE imaging is limited by their

dx.doi.org/10.1021/cm200241c |*Chem. Mater.* 2011, 23, 2860–2868

size. Moreover, the nanometric dimension of these droplets is consistent with possible smearing of the heat effect corresponding to their glass transition in the DSC thermogram.[34] Clearly, the droplet size would be critically dependent upon the relative magnitudes of the cooling rate versus the nucleation and growth rates of the droplet phases in these liquids. It should be noted here that the observation of two T_g values in the DSC thermogram of a glass by itself does not necessarily imply the presence of polyamorphic phases. Chemically phase separated glasses are typically characterized by more than one glass transition. Moreover, even for a homogeneous glass, an intervening partial crystallization event following the first glass transition may result in a sufficiently altered composition of the residual glass that can lead to a second glass transition. However, this is clearly not the case for the DSC thermogram of the sample with 30 mol % Y_2O_3 that displays a single T_g as discussed above.

The phenomenon of liquid−liquid phase transition and polyamorphism dates back to the thermodynamic description of a two-state liquid that was first proposed by Rapoport.[35,36] This two-state liquid model is based on a regular solution of the low- and high-density states coexisting in a liquid that incorporates an enthalpic mixing parameter U and is characterized by a critical temperature $T_c = U/2k_B$.[36] The magnitude of U is typically smaller than the latent heat of fusion, so T_c falls below the melting temperature. For temperatures below T_c, the free energy G has a double minimum that corresponds to the formation of two structurally and thermodynamically distinct but compositionally identical amorphous phases upon glass transition, one with a low density (LDA) and one with a high density (HDA). Consequently, polyamorphism is generally expected in the supercooled liquid state, with the low-density and high-density liquid components being separated by a density-driven liquid−liquid phase separation. Hence, the density-driven phase separation can be observed in the quenched glass only if T_c is substantially higher than T_g such that the droplet phase can nucleate and grow in the supercooled liquid state before these dynamical processes are arrested by glass transition. In this scenario, the presence of relatively large droplets in the glasses with 24 and 41 mol % Y_2O_3 and that of significantly smaller droplets in the glass with 30 mol % Y_2O_3 may indicate that the difference between T_c and T_g goes through a minimum in these glasses near an Y_2O_3 content of ∼30 mol %, provided the cooling rates of these samples are identical. On the other hand, it is also quite probable that the nucleation and growth rates of the droplet phases are strongly dependent on composition in these Y_2O_3−Al_2O_3 liquids.

One of the most elusive problems in the fundamental understanding of polyamorphism in the Y_2O_3−Al_2O_3 system is related to the current lack of knowledge about the differences in the atomic structures of these droplet and matrix glassy phases, i.e., the HDA and LDA phases that ultimately give rise to the density differences. Neutron or X-ray diffraction experiments are not very useful in this regard because one can obtain only spatially averaged structural information with these techniques. Furthermore, spatially resolved Raman spectra of the droplet and matrix glassy phases were not able to reveal differences between the two phases.[23] NMR spectroscopy can be a valuable technique in this regard because these spectra often allow direct structural interpretation of short-range order in glasses. The ^{27}Al MAS and 3QMAS NMR spectra of Y_2O_3−Al_2O_3 glasses as reported here (Figures 5 and 6) and in previous studies indicate the presence of Al^{IV}, Al^{V}, and Al^{VI} structural units in all glasses. However, such spectra do not reveal significant a compositional dependence of the chemical shift and electric field gradient parameters as well as of the relative fractions of these Al species[15] while the average densities of these glasses change significantly with composition (Figure 1). Previous ^{27}Al NMR studies conducted at high field indicated that the ratio of Al^{IV} to Al^{V} and Al^{VI} is approximately 65:35 irrespective of the chemical composition.[15] Therefore, it is clear that the variation in the bulk densities of these glasses is not controlled by the Al speciation in the structure. This result is not entirely surprising considering the fact that Y is significantly heavier than Al is likely to be responsible for the observed trend of density increase with an increase in Y_2O_3 content (Figure 1). Unfortunately, similar conclusions cannot be directly drawn for the density differences between the LDA and HDA phases without conducting spectroscopic measurements on isolated phases.

In contrast with the ^{27}Al NMR spectra, the structural interpretation of the ^{89}Y MAS NMR spectra of these glasses is not straightforward and requires careful consideration of the chemical shift systematics of ^{89}Y in crystalline yttrium aluminates and in other relevant crystal structures. Previous ^{89}Y NMR spectroscopic studies of yttrium aluminate crystals have reported isotropic chemical shifts (δ_{iso}) of 222 and 215 ppm for the eight-coordinated Y sites (Y^{VIII}) in crystalline YAG ($Y_3Al_5O_{12}$ with 37.5 mol % Y_2O_3) and $YAlO_3$ (50 mol % Y_2O_3), respectively.[13,37] On the other hand, the δ_{iso} values for seven- and six-coordinated Y (Y^{VII} and Y^{VI}) sites in $Y_4Al_2O_9$ (66.67 mol % Y_2O_3) are located near 190 and 220 ppm, respectively.[13] Detailed ^{89}Y NMR spectroscopic studies of fluorite-structured Y-doped ZrO_2 and CeO_2 have demonstrated that the ^{89}Y NMR chemical shift is a sensitive function of the coordination number of Y as well as of the field strength of the next-nearest neighbor cations.[38,39] For example, in Y-doped ZrO_2, the ^{89}Y NMR isotropic chemical shifts of ∼90, 200, and 300 ppm correspond to eight-, seven-, and six-coordinated Y, respectively. On the other hand, in Y-doped CeO_2, the eight-, seven-, and six-coordinated Y sites are characterized by δ_{iso} values that are shifted to lower frequencies of ∼0, 100, and 200 ppm, respectively. The field strengths, expressed in the form of charge:radius ratio, for eight-coordinated Ce^{4+} and Zr^{4+} ions are 4.12 and 4.76, respectively. Therefore, the ^{89}Y isotropic chemical shifts of the Y sites move to lower frequencies with an increasing Y coordination number and/or with decreasing field strengths of the next-nearest neighbor cations. Consequently, the width of the broad ^{89}Y resonance in Figure 7 may be partially related to the structural disorder resulting from a corresponding distribution of next-nearest neighbor Al^{3+} ions with different coordination numbers and hence with different field strengths. It may be noted here that the charge:radius ratios of Al^{3+} ions in four-, five-, and six-coordinated cases are 7.75, 6.25, and 5.60, respectively. Considering the chemical compositions of the Y_2O_3−Al_2O_3 glasses studied here, the next-nearest neighbor cation environments around Y in these glasses are expected to be either similar to or more Al-rich than that in the structure of crystalline YAG. As noted earlier, the δ_{iso} for the Y^{VIII} sites in YAG and in $YAlO_3$ is in the range of 215−222 ppm. The field strengths of Al^{3+} ions that are four-, five-, and six-coordinated vary within the range of ∼5−8 and are significantly higher than values near ∼3, characteristic of the field strengths of Y^{3+} that is six-, seven-, or eight-coordinated. Hence, the replacement of Y next-nearest neighbors with Al in Y_2O_3−Al_2O_3 glasses with an Al concentration higher than that of YAG is expected to result in a high-frequency shift of the δ_{iso} to values higher than ∼220 ppm for the Y^{VIII} sites.

The broad ^{89}Y resonance centered around 220 ppm (Figure 7) in the ^{89}Y MAS NMR spectrum of the glass with 41 mol % Y_2O_3 corresponds predominantly to the presence of Y^{VIII} sites in this glass that are similar to those in YAG, albeit with significant structural disorder. This result is not unexpected considering the compositional similarity between this glass and YAG. On the other hand, the center of gravity of the broad ^{89}Y resonance shifts progressively to a lower frequency with an increasing Al content to near 175 ppm for the glass with 24 mol % Y_2O_3. As discussed above, this frequency shift cannot be ascribed to an increase in the relative concentration of Al^{3+} cations in the next-nearest neighbor environment of the Y^{VIII} sites. Therefore, such a shift most likely corresponds to an increase in the average coordination number of Y to a value somewhat higher than eight in glasses with 30 and 24 mol % Y_2O_3.

It is instructive in this regard to employ simple bond valence theory to understand the local polyhedral connectivities and the effect of increasing Al on the Y coordination environments that may be present in these glasses. In the crystal structure of YAG, each oxygen is shared by two YO_8 polyhedra, one AlO_4 polyhedron, and one AlO_6 polyhedron, resulting in a 60:40 Al^{IV}:Al^{VI} ratio that is similar to the Al^{IV}:Al^{V} and Al^{VI} ratio of ~65:35 that is characteristic of the $Y_2O_3-Al_2O_3$ glasses. Therefore, considering the similarity between YAG and the glass with 41 mol % Y_2O_3 in their Y coordination environments, bond valence theory can be used to predict that each oxygen atom in the YO_8 polyhedron in the glass will be shared by another YO_8 polyhedron and one AlO_4 polyhedron and one AlO_5 or AlO_6 polyhedron for optimal charge balance. On the other hand, in glasses with Al contents higher than that of YAG, one expects each oxygen to be shared on average by more than two AlO_x ($x = 4$, 5, or 6) polyhedra with a similar average Al^{IV}:Al^{V} and Al^{VI} ratio of ~65:35 irrespective of glass composition. This is expected to result in a partial positive charge contribution to oxygen from the Al^{3+} ions that is larger than that characteristic of YAG. Such a change in the polyhedral connectivity would require an increase in the coordination number of Y so that the partial positive charge contribution to oxygen from the Y^{3+} ions decreases to compensate for the contribution from the Al^{3+} ions. As mentioned earlier, this scenario is consistent with the ^{89}Y MAS NMR results that indicate an increase in the average coordination number of Y with an increasing Al content in the $Y_2O_3-Al_2O_3$ glasses. Previous studies based on X-ray and neutron diffraction and reverse Monte Carlo simulation suggested an average coordination number close to seven for Y in these glasses with Y_2O_3 contents ranging between 20 and 27 mol % or approximately six for compositions near that of YAG with some small concentration of Y that is eight-coordinated.[12,20,40] These coordination numbers are significantly lower than an average value of approximately eight or slightly higher as indicated by the ^{89}Y NMR spectra reported here. Such a discrepancy may possibly originate from the extensive overlap between the Y−O and O−O correlations in the experimental radial distribution functions of these glasses that makes an accurate determination of the Y−O coordination number difficult. However, it is noteworthy that these diffraction studies indicate an increase in the Y−O coordination number with an increasing Al content in these glasses. This trend is qualitatively similar to the findings reported in this study on the basis of the ^{89}Y NMR results.

Although an exact assignment of the narrow ^{89}Y resonance near 75 ppm in Figure 7 to a specific Y coordination environment in the glass structure is not possible at this stage, as mentioned above the magnitude of the frequency shift of this peak is consistent with a coordination number of nine (i.e., Y^{IX} sites). Alternatively, it is possible that this narrow peak at 75 ppm also corresponds to Y^{VIII} sites but in a structure that is locally substantially different from that of YAG. The ^{89}Y NMR line widths in these materials are expected to be controlled by inhomogeneous broadening resulting from glassy structural disorder. Therefore, irrespective of whether this narrow peak represents Y^{VIII} sites or Y^{IX} sites, it is clear that such sites exist in regions in the glass structure where the degree of short-range order around Y atoms is significantly higher than the degree of order of the rest. Considering the higher relative fraction of the broad ^{89}Y resonance in the ^{89}Y MAS NMR spectra in Figure 7, it is sensible to associate the narrow and broad ^{89}Y NMR resonances with the droplet and matrix phases, i.e., with regions of lower and higher density, respectively, in these glasses. The HDA phase is expected to be the dominant phase in these glasses considering the fact that this phase is stable at low temperatures near glass transition. However, on the other hand, if the formation of the HDA phase when the liquid is cooled is controlled by nucleation and growth, then it may correspond to the minor droplet phase. Therefore, a conclusive statement regarding the assignment of the two ^{89}Y NMR resonances to the HDA and LDA phases cannot be made without taking spectroscopic measurements on isolated phases.

Typically, in crystalline materials, the NMR line widths increase with decreasing particle size in the nanometer regime because of increasing structural disorder and strain associated with the large increase in the surface area in nanoparticles.[40] However, the width of the narrow ^{89}Y resonance near 75 ppm in Figure 7 is relatively insensitive to the size of the droplets that varies from several nanometers to several micrometers in these glasses. One possible explanation for this apparent discrepancy may be associated with the fact that unlike crystals the droplets are amorphous without any long-range structural periodicity and the short-range structure is rather insensitive to the size of these droplets. The presence of both the narrow and the broad ^{89}Y resonances in the ^{89}Y MAS NMR spectra of glasses with 24, 30, and 41 mol % Y_2O_3 would then indicate that both LDA and HDA phases are present in all three glasses. This is consistent with the direct observation of the droplet and matrix phases in the BSE and TEM images of these glasses. An assignment of the narrow ^{89}Y NMR resonance to the LDA phase would imply a higher degree of short-range structural order around Y atoms in this phase and hence lower frozen-in configurational entropy compared to that in the HDA phase. This scenario would be consistent with similar suggestions made in the literature by McMillan, Wilding, and co-workers on the basis of the X-ray diffraction results.[41] Moreover, the higher molar volume and lower entropy of the LDA phase compared to those of the HDA phase would be expected to result in a negative Clapeyron slope ($dP/dT = \Delta S/\Delta V$) associated with the phase transition, where ΔS and ΔV are the associated changes in entropy and volume, respectively.

SUMMARY

The microstructures of $Y_2O_3-Al_2O_3$ glasses are investigated in relation to polyamorphism. The Al speciation in these glasses is nearly independent of composition, and Al atoms are mostly four-coordinated with low concentrations of five- and six-coordinated forms. On the other hand, nearly 70% of the Y atoms in these glasses are eight-coordinated while the rest of the

Y atoms are nine-coordinated. All $Y_2O_3-Al_2O_3$ glasses in this composition range are characterized by the coexistence of polyamorphic HDA and LDA phases. These two phases are compositionally identical, differ in the density, degree of short-range structural order in the Y coordination environment, and Y−O coordination number, and are characterized by distinct glass transition temperatures.

■ ACKNOWLEDGMENT

N.K.N. thanks the International Materials Institute for New Functionality in Glass (IMI-NFG, supported by National Science Foundation Grant DMR 0844014) for financial support during his stay at the University of California. We express our gratitude to Drs. Erica Gjersing and Ping Yu for help with collection of the NMR spectra and Mr. Fred Hayes for his help with TEM. The financial support to N.K.N. and G.N.P. from the Executive Board of FORTH is acknowledged. S.S. was supported by National Science Foundation Grant DMR0906070.

■ REFERENCES

(1) Brusset, H.; Gillier-Pandraud, M. H.; Saine, M. C. *Mater. Res. Bull.* **1975**, *10*, 481.
(2) Kahn, A.; Lejus, A. M.; Madsac, M.; Théry, J.; Bernier, J. C. *J. Appl. Phys.* **1981**, *52*, 6864.
(3) Weber, J. R. K.; Felten, J. J.; Cho, B.; Nordine, P. C. *Nature* **1999**, *393*, 769.
(4) Arsenev, P. A.; *Phys. Status Solidi A* **1975**, *28*, 81.
(5) Cockayne, B. *J. Less-Common Met.* **1985**, *114*, 199.
(6) Cockayne, B.; Lent, B. *J. Cryst. Growth* **1979**, *46*, 371.
(7) Gervais, M.; Le Floch, S.; Rifflet, J. C.; Coutures, J.-P.; Coutures, J. *J. Am. Ceram. Soc.* **1987**, *256*, 427.
(8) Aasland, S.; McMillan, P. F. *Nature* **1994**, *369*, 633.
(9) Weber, J. K. R.; Abadie, J. G.; Hixson, A. D.; Nordine, P. C.; Jerman, G. A. *J. Am. Ceram. Soc.* **2000**, *83*, 1868.
(10) Wilding, M. C.; McMillan, P. F. *J. Non-Cryst. Solids* **2001**, *293−295*, 357.
(11) Wilding, M. C.; McMillan, P. F.; Navrotsky, A. *Phys. Chem. Glasses* **2002**, *43*, 306.
(12) Wilding, M. C.; McMillan, P. F.; Navrotsky, A. *Phys. A (Amsterdam, Neth.)* **2002**, *314*, 379.
(13) Florian, P.; Gervais, M.; Douy, A.; Massiot, D.; Coutures, J. P. *J. Phys. Chem. B* **2001**, *105*, 379.
(14) Nagashio, K.; Kuribayashi, K. *J. Am. Ceram. Soc.* **2002**, *85*, 2353.
(15) Tangeman, J. A.; Phillips, B. L.; Nordine, P. C.; Weber, J. K. R. *J. Phys. Chem. B* **2004**, *108*, 10663.
(16) Wilson, M.; McMillan, P. F. *Phys. Rev. B* **2004**, *69*, 054206.
(17) Wilding, M. C.; Benmore, C. J.; McMillan, P. F. *J. Non-Cryst. Solids* **2002**, *297*, 143.
(18) Wilding, M. C.; Wilson, M.; McMillan, P. F. *Philos. Trans. R. Soc. London, Ser. A* **2005**, *363*, 589.
(19) Cristiglio, V.; Hennet, L.; Cuello, G. J.; Pozdnyakova, I.; Johnson, M. R.; Fischer, H. E.; Zanghi, D.; Vu Van, Q.; Wilding, M. C.; Greaves, G. N.; Price, D. L. *J. Phys.: Condens. Matter* **2007**, *19*, 41505.
(20) Weber, R.; Benmore, C. J.; Siewenie, J.; Urquidi, J.; Key, T. S. *Phys. Chem. Chem. Phys.* **2004**, *6*, 2480.
(21) Du, J.; Benmore, C. J.; Corrales, R.; Hart, R. T.; Weber, J. K. R. *J. Phys.: Condens. Matter* **2009**, *21*, 205102.
(22) Skinner, L. B.; Barnes, A. C.; Salmon, P. S.; Crichton, W. A. *J. Phys.: Condens. Matter* **2008**, *20*, 205103.
(23) McMillan, P. F.; Wilding, M. C. *J. Non-Cryst. Solids* **2008**, *354*, 1015.
(24) Greaves, G. N.; Wilding, M. C.; Fearn, S.; Langstaff, D.; Kargl, F.; Cox, S.; Vu Van, Q.; Majérus, O.; Benmore, C. J.; Weber, R.; Martin, C. M.; Hennet, L. *Science* **2008**, *322*, 566.
(25) Barnes, A. C.; Skinner, L. B.; Salmon, P. S.; Bytchkov, A.; Pozdnyakova, I.; Farmer, T. O.; Fischer, H. E. *Phys. Rev. Lett.* **2009**, *103*, 225702.
(26) Greaves, G. N.; Wilding, M. C.; Fearn, S.; Kargl, F.; Hennet, L.; Bras, W.; Majérus, O.; Martin, C. M. *J. Non-Cryst. Solids* **2009**, *355*, 715.
(27) McMillan, P. F. *J. Mater. Chem.* **2004**, *14*, 1506–1512.
(28) Kalampounias, A. G.; Papatheodorou, G. N. In *13th International Symposium on Molten Salts*; Trulove, P. C., De Long, H. C., Mantz, R. A., Stafford, G. R., Matsunago, M., Eds.; The Electrochemical Society: Pennington, NJ, 2002; p 485, PV 02-19.
(29) Baltisberger, J. H.; Xu, Z.; Stebbins, J. F.; Wang, S. H.; Pines, A. *J. Am. Chem. Soc.* **1996**, *118*, 7209.
(30) Schaller, T.; Stebbins, J. F. *J. Phys. Chem. B* **1998**, *102*, 10690.
(31) Amoureaux, J.-P.; Huguenard, C.; Engelke, F.; Taulelle, F. *Chem. Phys. Lett.* **2002**, *356*, 497.
(32) Johnson, B. R.; Kriven, W. M. *J. Mater. Res.* **2001**, *16*, 6.
(33) McMillan, P. F.; Wilson, M.; Wilding, M. C. *J. Phys.: Condens. Matter* **2003**, *15*, 6105–6121.
(34) Trofymluk, O.; Levchenko, A. A.; Navrotsky, A. *J. Chem. Phys.* **2005**, *123*, 194509.
(35) Rapoport, E. *J. Chem. Phys.* **1967**, *46*, 2891.
(36) Rapoport, E. *J. Chem. Phys.* **1967**, *48*, 1433.
(37) Dupree, R.; Smith, M. E. *Chem. Phys. Lett.* **1988**, *148*, 41.
(38) Kawata, K.; Maekawa, H.; Nemoto, T.; Yamamura, T. *Solid State Ionics* **2006**, *177*, 1687.
(39) Kim, N.; Stebbins, J. F. *Chem. Mater.* **2007**, *19*, 5742.
(40) Jain, P.; Avila-Paredes, H. J.; Gapuz, C.; Sen, S.; Kim, S. *J. Phys. Chem. C* **2009**, *113*, 6553.
(41) McMillan, P. F.; Wilson, M.; Wilding, M. C.; Daisenberger, D.; Mezouar, M.; Greaves, G. N. *J. Phys.: Condens. Matter* **2007**, *19*, 415101.